Accurate determination of electrical conductance in carbon nanostructures

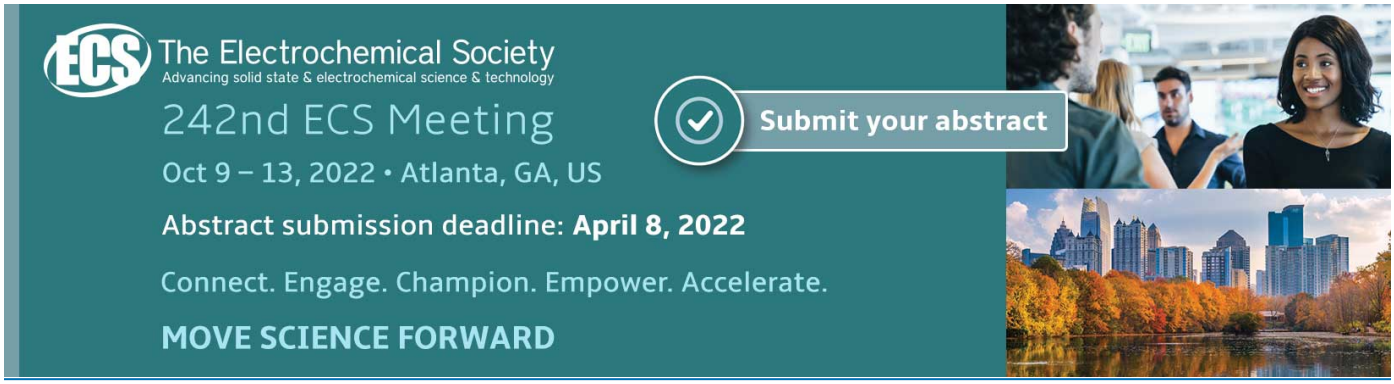

Materials Research Express

PAPER

Accurate determination of electrical conductance in carbon nanostructures

Mattias Flygare and Krister Svensson

Department of Engineering and Physics, Karlstad University, SE-651 88 Karlstad, Sweden

E-mail: krister.svensson@kau.se

Keywords: carbon nanotubes, electrical conductivity, transmission electron microscopy

OPEN ACCESS

RECEIVED
14 December 2021

REVISED
6 March 2022

ACCEPTED FOR PUBLICATION
15 March 2022

PUBLISHED
31 March 2022

Abstract

Electrical characterization of nanostructures, such as nanotubes and wires, is a demanding task that is vital for future applications of nanomaterials. The nanostructures should ideally be analyzed in a free-standing state and also allow for other material characterizations to be made of the same individual nanostructures. Several methods have been used for electrical characterizations of carbon nanotubes in the past. The results are widely spread, both between different characterizations methods and within the same materials. This raises questions regarding the reliability of different methods and their accuracy, and there is a need for a measurement standard and classification scheme for carbon nanotube materials. Here we examine a two-probe method performed inside a transmission electron microscope in detail, addressing specifically the accuracy by which the electrical conductivity of individual carbon nanotubes can be determined. We show that two-probe methods can be very reliable using a suitable thermal cleaning method of the contact points. The linear resistance of the outermost nanotube wall can thus be accurately determined even for the highest crystallinity materials, where the linear resistance is only a few kΩ/μm. The method can thereby by used as a valuable tool for future classification schemes of various nanotube material classes.

1. Introduction

Carbon nanotubes have promising electrical applications due to their high electrical conductivity and high current-carrying capabilities. These properties are highly sensitive to the quality of the material and there is a need for accurate characterization of the electrical properties and their dependence on material production methods, post-production treatments and final material quality. Several methods have been tried in the past, with a wide spread in the results between them. This demonstrates the need for standardized characterization methods and material standards for commercially produced carbon nanotube materials, in order to fully exploit these materials in future applications.

Early methods for electrical characterization involved prepatterned electrodes on an insulating substrate followed by carbon nanotube deposition from solution. By chance, there would be nanotubes bridging the electrodes and thus enabling electrical characterization. Making good electrical contacts proved, however, to be a major challenge, and the total resistance would typically be in the MΩ range [1]. This was further reduced by electron-beam irradiation, similar to 'spot-welding', taking resistances into the kΩ range, and the effect was believed to be related to an improved electrical contact rather than a modification of the nanotube structure itself [1, 2]. Using this method, estimates of the linear resistance, which is resistance per nanotube length, were found in the range of 1.4–10.4 kΩ/μm.

Another promising route is to deposit the nanotubes first and then lay down electrodes, using e-beam lithography, on top of the tubes. The method has found contact resistances in the range 0.1–20 kΩ shortly after sample preparation, while the contacts are lost within a few weeks of storage [3]. The total resistance in two point measurements of MWCNTs have been found to be in the range of 5–30 kΩ [4]. The fabrication method will also allow for multiple contacts and four probe measurements, or even up to 11 electrodes [5]. With multiple

electrodes one can exclude the contact resistance and access the electrical resistance vs nanotube length, and values in the ranges of 6–25 kΩ/μm [5] and 0.2–86 kΩ/μm [6] have been reported. Other measurements, including estimates of band gaps, display similarly large spread is the data [7]. Furthermore, such methods are limited to electrical characterization and will not provide other valuable information, such as accurate diameter measurements and the number of walls.

Other ways to characterize nanotubes involve movable probes together with *in situ* scanning electron microscopes (SEM). With this method, the nanotubes can either be supported by an insulated substrate or free-standing in vacuum. For supported tubes there is a risk of deforming the tubes at the contact, while free-standing tubes can be contacted without also exerting unnecessary high forces. The limited vacuum conditions in the SEM will however give unwanted electron beam induced depositions (EBID), commonly in the form of amorphous carbon buildup from the presence of hydrocarbons in the background pressure of the chamber [8]. Any surface that is exposed by the electron beam during imaging is thereby covered by an amorphous carbon layer, thus obscuring the inherent nanotube properties. The effect can be reduced if only low magnifications are used, or the nanotubes are heated via Joule heating [9]. The SEM images lack other information, such as the number of tube walls which requires subsequent analysis of the same structure by using transmission electron microscopy (TEM).

Free-standing tubes have been examined by dipping carbon nanotube samples into a liquid metal, such as mercury, with an assumption that the contact position varies with the dipping length. The experiments showed almost no dependence between dipping length and resistance, with the conclusion that the nanotubes are quantum conductors over several micrometers even at room temperature [10]. Unexpectedly however, similar results were shown for several different materials [11, 12], and even for lower quality CNTs made in CVD processes [13]. A serious flaw in the method was later revealed, showing that the nanotubes may not actually penetrate the Mercury liquid, but instead the surface of the Mercury is deformed [14–16]. The small changes in resistance would then merely reflect resistance changes at the same fixed contact point as the pressure towards the liquid surface was varied [14].

Studies have also been performed inside TEM, where the better vacuum and image resolution has an advantage over SEM studies. Here the risk of EBID can be greatly reduced by using liquid nitrogen cooling traps near the sample region. TEM will also allow for structural characterization, such as the number of walls and the crystallinity of the material. The method relies on resistive heating of the contact points, in order to remove residual contaminations of the nanotubes surface, which can be done at low enough currents in order to avoid thermal modifications to the tubes themselves [17–19]. The obtained linear resistance shows a spread in the range 3–300 kΩ/μm, still a fairly large spread, but one which can be linked to individual differences in the nanotubes that may be characterized in the TEM alongside the electrical characterizations [19].

Here we investigate *in situ* TEM characterizations in more detail and focus on the accuracy of the electrical characterization. We find that the electrical contacts are highly reproducible, using Joule heating, and that the linear resistivity can indeed be determined with high accuracy, following a provided measurement scheme.

2. Experimental details

The TEM sample holder was fitted with a scanning tunneling microscope (STM) with a compact, three-dimensional, inertial slider design [20], to be used for electrical characterization. A tip mounted in the STM can then be moved during regular TEM operation. The probe tip was used to apply voltage bias ramps to the sample specimen as well as holding a stationary voltage bias while measuring the induced current. As electrodes, two types of tips were used, including commercially available tungsten tips from NaugaNeedles™ coated with platinum (NN-WNP-Pt), and manually cut gold wires with a diameter of 0.25 mm.

Measurements were performed at room temperature using a JEOL (JEM 2100) TEM equipped with a LaB_6 cathode and a digital camera from Gatan (SC1000 Orius). The main column was pumped with a turbo pump and while using the anti-contamination device cooled with liquid nitrogen the base pressure was around 7×10^{-8} mbar. In order to avoid electron beam induced knock-on damages of the samples the acceleration voltage was kept at 90 kV [21].

Selected area electron diffraction (SAED) was used for the analysis of crystallinity, as described in [22]. Oriented single-crystal gold foils induced to grow in a (100) orientation obtained from Electron Microscopy Sciences (EMS Catalog #80038) with lattice plane spacings of 0.204 nm, 0.144 nm and 0.102 nm, were used for calibrations of the diffraction pattern scale and for estimating the intrinsic broadening of the diffraction patterns due to the angular spread in the TEM beam.

Multi-walled carbon nanotubes (MWCNTs) grown by arc-discharge obtained from Professor Hui-Ming Cheng at the Institute of Metal Research, Chinese Academy of Sciences, Shenyang, China were used. The outer diameter of all tubes measured was 7–25 nm with a mean value of 14 nm. A small amount of the sample was

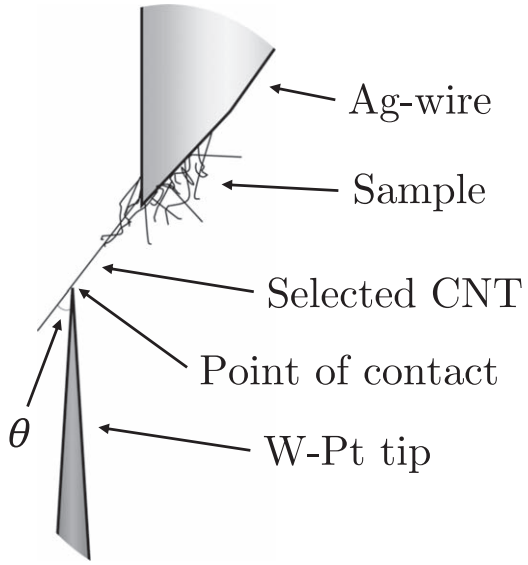

Figure 1. A schematic of the experiment showing the silver wire holding the sample specimen, and the platinum coated tungsten probe tip, as the tip makes contact with a CNT.

glued to a sharpened silver wire with electrically conductive silver epoxy (Chemtronics CW2400), and the wire was mounted in the sample holder adjacent to the probe tip.

3. Results and discussion

3.1. Sample preparation and probe tip

Samples were prepared both by dissolving the bulk powder in dichloroethane with sonication, and by simply scraping off and crushing the sample particles into the finest powder possible. The two methods of preparation had similar results, and the latter one was preferred to minimize the risk of damage, accidental doping or contamination from solvent or sonication [23, 24].

A small part of the prepared sample was spread out onto a glass surface. A thin silver wire of diameter 0.25 mm was cut to have a sharp edge (about 45°) and dipped into electrically conductive silver epoxy. The edge of the wire covered with epoxy was lowered towards the glass containing the sample while observed with an optical microscope, coming in towards a specimen particle from the side, until the particle was glued to the wire. Contact was made using minimal force to ensure the specimen was not embedded in glue, preventing access to protruding CNTs.

The choice of probe electrode tip-material was made to obtain a stiff and thin shaped tip with a relatively low and reproducible contact resistance [25]. A tungsten tip coated with platinum and a gold wire were both tested. The thin gold wire was manually cut to a sharp edge, and would give a reliable and low contact resistance. The wire was however difficult to cut sharp enough, and was easily deformed. The tungsten tip was found to have a very reliable and sharp shape, a high bending stiffness, gave a low and reliable contact resistance, and was used for all measurements in the study.

If needed, before TEM testing, both sample wire and probe tip was rotated after initial mounting, aided by using an optical microscope.

3.2. Tube selection

Using TEM imaging, a suitably protruding and free-hanging CNT was selected from the sample specimen. In order to have enough geometrical access to take a series of measurements along the tube's length, it was found that the angle θ between the tube and probe tip within the TEM imaging plane should preferably exceed 30°, as shown in figure 1.

For smaller angles, the tube could sometimes be approached by the probe tip from above or below, with respect to the imaging plane, however this was avoided since it may add uncertainty when localizing the point of contact. To optimize the geometry for probe approach, the sample and probe was rotated around the axis going through them both by tilting the TEM sample holder. The probe tip was further adjusted in three dimensions by controlling the probe piezo.

Tubes that had adjacent tubes or other sample material touching or blocking access to the tube were avoided, using only free-hanging and uncontaminated tubes for measurements of linear resistance in this study.

3.3. Contact between probe tip and tube

The tip was moved to the same height as the tube using the probe piezo, then slowly towards the tube's outermost wall, until contact was made. A snap-in effect often occurred when a gap of about 1 nm remained between the tube and tip, where the gap quickly closed due to movement of the tube, driven by van der Waals forces.

Upon contact, the connected probe and tip were carefully moved back to the position where the tube was freely hanging, in order to reduce the risk of tension in the CNT, as well as minimizing unnecessary pressure exerted on the tube by the probe tip, which may affect contact resistance. Bending the tube by applying force with the probe tip was tested, which showed resistance measurements remaining constant and stable, indicating that the method is fairly insensitive to unnecessary pressure from the probe. Nevertheless, pressure applied by the probe on the tube was minimized.

Contact between the probe tip and tube was made on the side and not on the end of the MWCNT. Such end-contact was avoided partly due to the risk of unintentionally making contact between the electrode and multiple tube walls [26], as well as eliminating the possibility of the more conductive atomic bonding at the tube end, compared to the less conductive van der Waals bonds on the side of the tubes. Both possibilities may lead to a significantly lower contact resistance [25, 27, 28], and end-contact electrical measurements are thus hard to interpret and not usable in the context of the linear resistance in the outermost tube wall.

3.4. Annealing using joule heating

The TEM electron beam was directed away from the tip and sample when applying electrical bias to the probe, in order to prevent beam-induced damage and hydrocarbon deposition and to reduce the risk of electron beam influence on electrical measurements.

Low bias measurement immediately after making contact with a tube resulted in a relatively high and unstable contact resistance. To reduce contact resistance and minimize variance between different points of contact, annealing by Joule heating was implemented [8, 17]. A voltage bias of 2 V with induced currents of around 30–100 μA was used, without damage to the sample specimen. The current/bias limit for MWCNT failure or deformation will likely depend on crystallinity, diameter and number of walls, but was not explored in this study. The anneal was divided into three phases; increase, hold and decrease, where bias was increased linearly to 2 V during 2 seconds, held for 10 seconds, and finally reduced back to 0 V during 2 seconds. An example of the resulting current during such a treatment is shown in figure 2.

A statistical analysis including 90 different annealing instances showed that 81% of the anneals had a lower resistance in the last two seconds of the annealing hold phase compared to the first two, with a mean drop of 3.3%. The drop in resistance decreases for each two second interval to the next in the 10 second hold, and was on average 0.1% going from time span 6–8 s. to 8–10 s. Similarly, some variance in resistance is present throughout the hold phase, but drops drastically after the first few seconds. In the first two second interval the standard deviation from the mean was found to be over 3 kΩ, while for all subsequent two second intervals of the hold phase, the standard deviation was below 1 kΩ, as shown in figure 3. Excluding the first two seconds of the hold phase, the standard deviation of the remaining 8 seconds was 1.3 kΩ. The analysis shows that the contact resistance is initially high and unstable, as the example shows figure 2a, significantly lowered and stabilized by the end of the increasing phase of the anneal, and remains very stable after the first two seconds of the hold phase.

3.5. Point resistance measurements and linear resistance

For higher bias voltages, the current/voltage relationship becomes superlinear, as is shown in figure 2(b), due to MWCNT intershell conduction [5, 29]. To ensure outermost wall conduction was the dominating mode of electron transport, the bias voltage was kept below 5 mV for measurements of point resistance. An example of such a measurement can be found in [19] figure 2. The resistance was found to be ohmic at low bias after annealing, and the mean value of the differential resistance was calculated and used as the average measured resistance R_p of the point of contact.

The distance l_p, which is the distance between electrodes, was measured using TEM imaging for each point of contact. For the position of the electrode on one side, the point of probe/tube contact was used, shown as point 1 in figure 4. On the other side the tube's closest contact with the silver wire, conducting glue or other part of the sample in contact with the wire was used. The actual wire/tube contact was often obscured, in which case the point where the tube is no longer visibly free-hanging was used, shown as point 2 in figure 4.

The tip was slowly retracted from the tube wall until contact was broken, completing one cycle of point measurement. The sequence was repeated for each tube until a sufficiently large set of measurements was

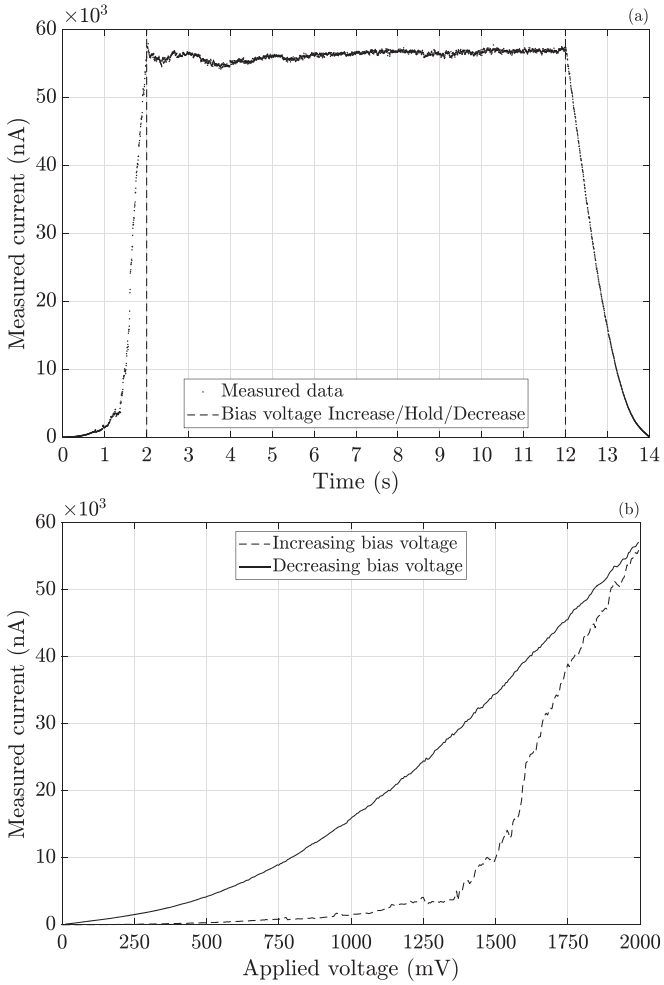

Figure 2. (a) Current plotted versus time for a typical anneal, where the bias was increased linearly to 2 V during 2 seconds, held for 10 seconds, and finally reduced back to 0 V during 2 seconds. (b) Current versus applied bias voltage for the same example, with both increasing and decreasing bias.

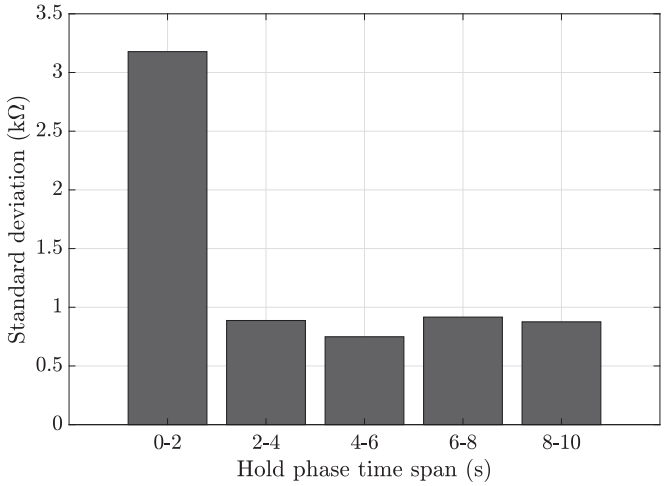

Figure 3. A statistical analysis, including 90 annealing instances, of the standard deviation from the mean resistance value during the hold phase of an anneal. The standard deviation is taken in two second intervals, for all 10 seconds of the hold phase.

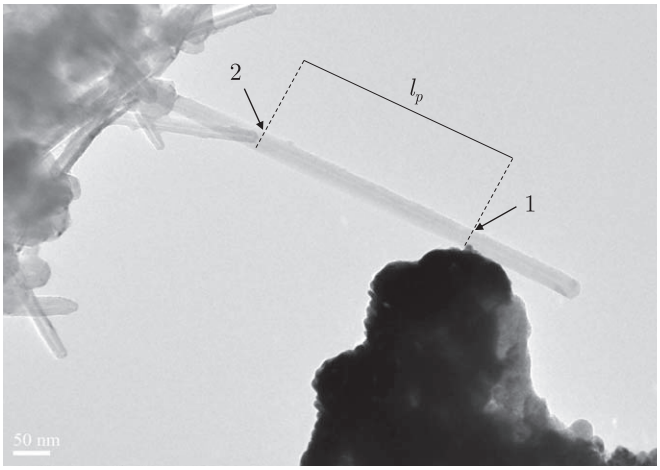

Figure 4. A TEM image picturing an example of a point measurement. The distance l_p was measured between point 1 where the probe tip is in contact with the tube, and point 2 where the tube is no longer visibly free-hanging.

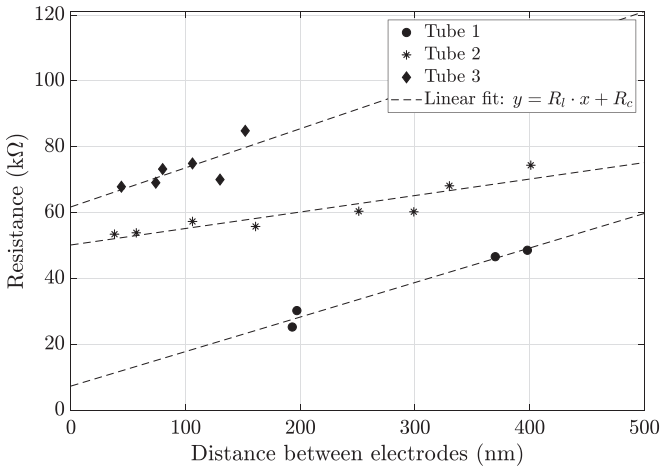

Figure 5. An example of linearisation to calculate R_b shown for three different CNTs. The slope of the respective linear fit corresponds to the tube's linear resistance R_l and the intersects can be taken as an upper bound for the contact resistance R_c.

obtained, taking into account the number of contact points, the range of l_p and the variance of each point measurement. R_p was fitted linearly versus l_p for each tube, assuming

$$R_p = R_l \cdot l_p + R_c, \tag{1}$$

where the fitting parameters R_l is the linear resistance of the specific section of tube in question and R_c represents the sum of all of the contact resistances between the main sample, the specific tube and the probe electrodes. An example of this is shown for three tubes in figure 5, and a more detailed description of this procedure can be found in [19].

The same point of reference for the electrode on the side of the sample holder wire, shown as point 2 in the example in figure 4, was used for all measurements of l_p related to a specific tube, only varying the position of the tip/tube contact, shown as point 1. Thus, the possible error in the approximation of l_p does not have an impact when characterizing linear resistance R_b, however it may affect the value for the tube's contact resistance R_c. The value calculated for R_c should therefore be interpreted as 'the constant part of all resistance measurements on the tube, including contact resistance of the electrodes', which can be used as a conservative upper bound for probe/tube contact resistance.

3.6. Standard deviation of point resistance measurements

In a statistical analysis including 82 points of resistance measurement it was found that 51% of values for R_p deviated less than 2 kΩ from the value predicted by R_l, 63% deviated less than 3 kΩ and 70% deviated less than 5 kΩ.

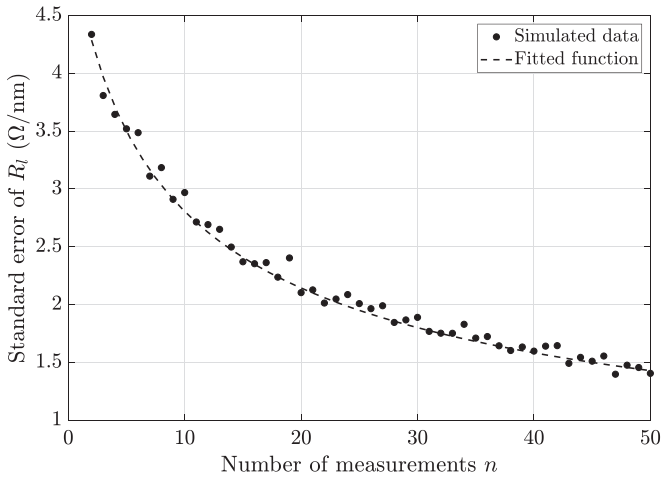

Figure 6. Each point is a simulated value, over 500 iterations, of the standard error of R_l given a constant standard deviation $\mathrm{SD}(R_p) = 3$ kΩ, for n points of measurement. Each point of measurement was distributed randomly over a length of $l_{\mathrm{tot}} = 1000$ nm. The dashed line corresponds to the fitted function in (2).

The standard deviation of R_p can also be estimated by using the 1.3 kΩ standard deviation of the last 9 seconds of the anneal hold phase, described in section 3.4. These uncertainties can be interpreted as an instability in contact resistance induced by Joule heating. For low bias, the contact resistance is completely stable, and the uncertainty in contact resistance is carried over from the preceding anneal.

The added variance found in the linear resistance analysis compared to the standard deviation in resistance found in the analysis of electrical annealing may have more than one cause. Inhomogeneity in the tubes may make the assumption of a linear resistance in the tube section less accurate. Contact resistance may also scale with the total measured resistance of R_p, making it larger for low bias measurements, and thus scaling the standard deviation up along with it. The median of the ratio between low bias measured resistance and the preceding high bias resistance measured while annealing was found to be about 2, which would scale standard deviation for low bias up to 2.6 kΩ. Conversely, a statistical analysis showed that there was no significant dependence between standard deviation and resistance magnitude during annealing hold phases, even though the span of annealing hold phase resistance was 20–120 kΩ, clearly overlapping the span of low bias measured resistance. Furthermore, no significant dependence between low bias resistance and deviation from R_l prediction was found. Thus the analysis points to measurements having an absolute variance, rather than relative. For the measurements of R_p in this study, we have estimated a standard deviation of 3 kΩ.

3.7. Measuring error of linear resistance calculations

For a given standard deviation of the measured point resistance R_p, denoted $\mathrm{SD}(R_p)$, we estimate the standard error of the calculated linear resistance R_l, here denoted $\mathrm{SE}(R_l)$. It is clear that $\mathrm{SE}(R_l)$ is proportional to $\mathrm{SD}(R_p)$ and inversely proportional to the total length of the CNT section being measured, denoted l_{tot}, which equates to the range of l_p. For large number of measurements n we also expect that $\mathrm{SE}(R_l)$ will be proportional to $1/\sqrt{n}$, however since in this situation n will be relatively small, it is important to estimate the dependence more accurately. We were able to show by simulating values of R_p, as shown in figure 6, that the standard error of R_l for small n is closely proportional to $1/\sqrt{n+4}$. This lead to a final empirical expression for the standard error in linear resistance given by

$$\mathrm{SE}(R_l) = 3.5 \cdot \frac{\mathrm{SD}(R_p)}{l_{\mathrm{tot}}{}^{*}\sqrt{n+4}}, \tag{2}$$

where $\mathrm{SD}(R_p)$ is in kΩ, l_{tot} is in μm and $n \geqslant 2$.

In the simulation that led to (2), each point measurement was placed on a normal (Gaussian) distribution around a 'true' value based on constant values for linear resistance and contact resistance, with a predetermined and constant standard deviation for each measured point. Each point of measurement was distributed randomly over a set length of tube. It is important to note that distributing the points equidistantly along the tube resulted in a slightly different expression for the standard error, however the choice to distribute points randomly was determined to correspond better to the actual measurements that were done for this article.

From (2) we see that measuring over twice the length halves the error, while it would take more than a quadrupling of the number of points of measurement to obtain the same effect. Both the length of measuring

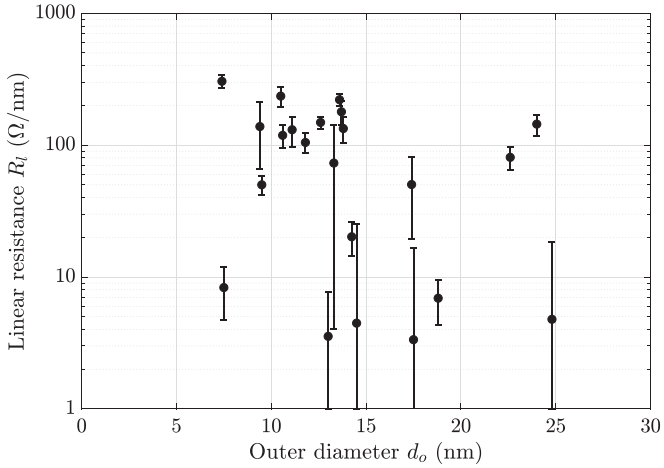

Figure 7. Linear resistance plotted versus the outer diameter d_o. The error bars indicate the estimated standard error of R_l which was calculated using (2).

and the number of point measurements are thus important to consider when attempting to minimize the standard error in linear resistance.

With measurement data from the dataset previously analyzed in [19] as input, the standard error for each individual value of R_l was calculated using (2). A plot of R_l versus outer tube diameter was created with error bars, shown in figure 7. The presence of the error bars strongly reinforces the results given in [19], being that tube diameter alone can not account for the spread in linear resistance seen in the data, even when taking into account the uncertainty in R_l indicated by the error bars. This is also consistent with the expressions for the number of electrically conducting channels of CNTs given in [30], which show that differences in conductivity due to chirality (i.e. tubes being metallic or semi-conducting) quickly diminish with increasing outer tube diameter. For diameters greater than about 10 nm the number of conducting channels (at room temperature and a bias voltage of 5 mV) will differ by about a factor of two or less, only contributing to a small part to the overall spread in linear resistance.

3.8. Mean crystallite grain size measurements

Following the method described in [22], SAED was used to determine the mean crystallite grain size L_a. A straight section of about 100 nm length (to fit the SAED aperture) from the electrical measurement region was selected and one or a series of diffraction images was captured. From this, the mean crystallite grain size L_a was calculated, and compared to the values for R_l.

As shown previously in [19], the spread in linear resistance R_l within a sample batch of CNTs is strongly correlated with the effective grain size L_a, and can be explained by a function that links R_l with grain size L_a for a given tube diameter. We are now able to show that this correlation holds even after taking into account the uncertainty in R_l as calculated before, indicated by the error bars in figure 8.

4. Conclusions

We have shown that two-probe methods can provide a very accurate measure of the linear resistance in carbon nanotubes. The method relies on thermal heating of the contacts, and especially the movable probe will need a thermal cleaning of each new point of contact. The accuracy and repeatability of the method is very high, and we find a standard deviation of around 3 kΩ for each point of contact. With a suitable number of contact points and a large enough spread in the positions, it is possible to characterize the linear resistance with a high accuracy even down to only a few kΩ/μm. We find that an apparent spread in the linear resistance values stems from differences in the material properties of individual tubes, rather than in the method itself. This was enabled by accompanying structural characterizations for each nanotube, which has proven to be a necessity for detailed studies of nanotube properties. We believe that the proposed method is accurate enough in order to serve as a first step towards a measurement standard, and hence as one of several tools needed for the characterization and classification of carbon nanotube materials.

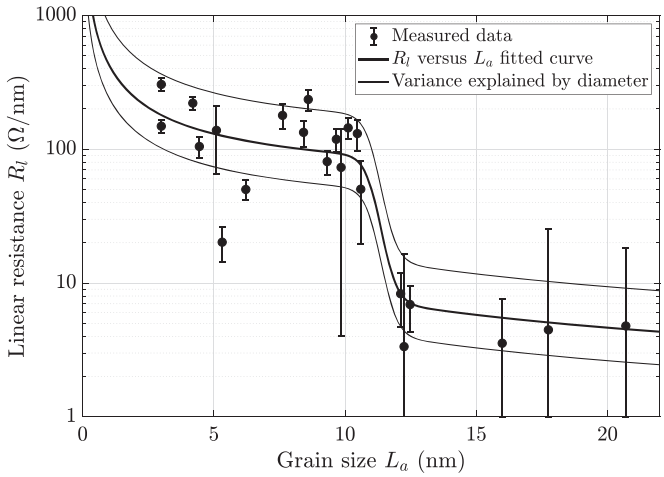

Figure 8. Linear resistance plotted versus the effective grain size L_a. The error bars indicate the estimated standard error of R_l which was calculated using (2). The fitted curve was plotted using the mean value of the outer diameter of the dataset, which was 14 nm. The curves shown above and below were plotted using the two extreme values of the outer diameter in the dataset, 7 nm and 25 nm respectively, to illustrate the variance related to tube diameter.

Acknowledgments

We are thankful to Prof. Hui-Ming Cheng at the Institute of Metal Research, Chinese Academy of Sciences, Shenyang, China, for supplying arc-discharge grown tubes.

Data availability statement

All data that support the findings of this study are included within the article (and any supplementary files).

ORCID iDs

Mattias Flygare https://orcid.org/0000-0002-5627-7637
Krister Svensson https://orcid.org/0000-0003-1711-5595

References

[1] Bachtold A, Strunk C, Schönenberger C, Salvetat J P and Forró L 1998 Electrical properties of single carbon nanotubes *AIP Conf. Proc.* 442, 65–8
[2] Bachtold A, Henny M, Terrier C, Strunk C, Schönenberger C, Salvetat J P, Bonard J M and Forró L 1998 Contacting carbon nanotubes selectively with low-ohmic contacts for four-probe electric measurements *Appl. Phys. Lett.* **73** 274–6
[3] Schönenberger C, Bachtold A, Strunk C, Salvetat J P and Forró L 1999 Interference and Interaction in multi-wall carbon nanotubes *Applied Physics A: Materials Science & Processing* **69** 283–95
[4] Bourlon B, Glattli D, Plaçais B, Berroir J, Miko C, Forró L and Bachtold A 2004 Geometrical Dependence of High-Bias Current in Multiwalled Carbon Nanotubes *Phys. Rev. Lett.* **92** 1–4
[5] Bourlon B, Miko C, Forró L, Glattli D C and Bachtold A 2004 Determination of the intershell conductance in multiwalled carbon nanotubes *Phys. Rev. Lett.* **93** 176806
[6] Ebbesen T W, Lezec H J, Hiura H, Bennett J W, Ghaemi H F and Thio T 1996 Electrical conductivity of individual carbon nanotubes *Nature* **382** 54–6
[7] Ahlskog M, Hokkanen M J, Levshov D, Svensson K, Volodin A and van Haesendonck C 2020 Individual arc-discharge synthesized multiwalled carbon nanotubes probed with multiple measurement techniques *Journal of Vacuum Science & Technology* B **38** 042804
[8] Chen Q, Wang S and Peng L M 2006 Establishing Ohmic contacts for in situ current-voltage characteristic measurements on a carbon nanotube inside the scanning electron microscope *Nanotechnology* **17** 1087–98
[9] Wei X, Chen Q, Peng L, Cui R and Li Y 2010 In situ measurements on individual thin carbon nanotubes using nanomanipulators inside a scanning electron microscope *Ultramicroscopy* **110** 182–9
[10] Poncharal P, Berger C, Yi Y, Wang Z L and De Heer W A 2002 Room temperature ballistic conduction in carbon nanotubes *J. Phys. Chem.* B **106** 12104–18
[11] Kajiura H, Nandyala A, Coskun U C, Bezryadin A, Shiraishi M and Ata M 2005 Electronic mean free path in as-produced and purified single-wall carbon nanotubes *Appl. Phys. Lett.* **86** 122106
[12] Kajiura H, Huang H and Bezryadin A 2004 Quasi-ballistic electron transport in double-wall carbon nanotubes *Chem. Phys. Lett.* **398** 476–9
[13] Kajiura H, Nandyala A and Bezryadin A 2005 Quasi-ballistic electron transport in as-produced and annealed multiwall carbon nanotubes *Carbon* **43** 1317–9

[14] Strand H U R 2007 Electron Transport characterization of multiwalled carbon nanotubes *Master of Science in Applied Physics* Chalmers Univeristy of Technology, Gothenburg, Sweden
[15] Strand H, Svensson K and Olsson E 2008 Measuring electrical properties of carbon nanotubes using liquid metal immersion, an in situ scanning electron microscopy study *EMC 2008 14th European Microscopy Congress 1 September 2008, Aachen, Germany (Springer Berlin Heidelberg, Berlin, Heidelberg)* 313-314
[16] Kobylko M, Kociak M, Sato Y, Urita K, Bonnot A M, Kasumov A, Kasumov Y, Suenaga K and Colliex C 2014 Ballistic- and quantum-conductor carbon nanotubes: a reference experiment put to the test *Phys. Rev.* B **90** 195431
[17] de Knoop L 2005 Investigation of iron filled multiwalled carbon nanotubes *Master of Science in Engineering Physics* Chalmers University of Technology, Gothenburg, Sweden
[18] de Knoop L, Svensson K, Pettersson H and Olsson E 2005 Extraction and Local Probing of Individual Carbon Nanotubes *AIP Conference Proceedings* 786, 118
[19] Flygare M and Svensson K 2021 Influence of crystallinity on the electrical conductivity of individual carbon nanotubes *Carbon Trends* **5** 100125
[20] Svensson K, Jompol Y, Olin H and Olsson E 2003 Compact design of a transmission electron microscope-scanning tunneling microscope holder with three-dimensional coarse motion *Rev. Sci. Instrum.* **74** 4945
[21] Meyer J C *et al* 2012 Accurate measurement of electron beam induced displacement cross sections for single-layer graphene *Phys. Rev. Lett.* **108** 196102
[22] Flygare M and Svensson K 2019 Quantifying crystallinity in carbon nanotubes and its influence on mechanical behaviour *Materials Today Communications* **18** 39–45
[23] Moonoosawmy K R and Kruse P 2008 To dope or not to dope: the effect of sonicating single-wall carbon nanotubes in common laboratory solvents on their electronic structure JACS **130** 13417–24
[24] Lu K L, Lago R M, Chen Y K, Green M L, Harris P J and Tsang S C 1996 Mechanical damage of carbon nanotubes by ultrasound *Carbon* **34** 814–6
[25] Wilhite P, Vyas A A, Tan J, Tan J, Yamada T, Wang P, Park J and Yang C Y 2014 Metal-nanocarbon contacts *Semicond. Sci. Technol.* **29** 054006
[26] Karita M, Asaka K, Nakahara H and Saito Y 2013 In situ TEM study on changes in structure and electrical conductance of carbon nanotube-gold contact induced by local joule heating *J. Mater. Sci.* **48** 936–40
[27] An L, Yang X and Chang C 2013 On Contact Resistance of Carbon Nanotubes *International Journal of Theoretical and Applied Nanotechnology* **1** 1–10
[28] Tersoff J 1999 Contact resistance of carbon nanotubes *Appl. Phys. Lett.* **74** 2122–4
[29] Agrawal S, Raghuveer M, Ramprasad R and Ramanath G 2007 Multishell Carrier Transport in Multiwalled Carbon Nanotubes *IEEE Trans. Nanotechnol.* **6** 722–6
[30] Kashcheyevs V, Tamburrano A and Sarto M S 2012 Quantum Transport and Current Distribution at Radio Frequency in Multiwall Carbon Nanotubes *IEEE Trans. Nanotechnol.* **11** 492–500